electronics

MDPI

Article

A Novel Epidemic-Based Video Diffusion Strategy Using Awareness of Sociality and Mobility in Wireless Networks

Shijie Jia [1], Ruiling Zhang [1,*], Xiaoyan Su [2] and Liuke Liang [2]

[1] Academy of Information Technology, Luoyang Normal University, Luoyang 471934, China
[2] Academy of Land and Tourism, Luoyang Normal University, Luoyang 471934, China
* Correspondence: ruilingzhang@163.com

Abstract: Social networks open up a new channel of video sharing and promote the scale and efficiency of video diffusion. Adjustable and scalable video diffusion is significant for the quality and performance of the service of video systems. In this paper, we propose a novel epidemic-based video diffusion strategy using awareness of sociality and mobility in wireless networks (EVDSM). EVDSM constructs a video diffusion model with the consideration of interest preference, social influence, and user mobility according to the roles and the propagation process of the Epidemic model. EVDSM designs an estimation method of interest preference according to content similarity and preference discrimination between videos; EVDSM designs an estimation method of user roles by investigation of interest preference and social influence to identify the video sharing behaviors of users and define the roles of users; EVDSM designs an estimation method of user mobility in terms of data transmission time and path structure stability. EVDSM proposes a control strategy of video diffusion, which formulates priority-based pairing between infectors and candidate infectors to achieve joint optimization of pairing success rate and delivery performance. The simulation results show how EVDSM achieves much better performance results in comparison with other state-of-the-art solutions.

Keywords: sociality-aware; mobility-aware; video diffusion; epidemic

Citation: Jia, S.; Zhang, R.; Su, X.; Liang, L. A Novel Epidemic-Based Video Diffusion Strategy Using Awareness of Sociality and Mobility in Wireless Networks. *Electronics* **2023**, *12*, 1305. https://doi.org/10.3390/electronics12061305

Academic Editor: Dimitris Kanellopoulos

Received: 15 February 2023
Revised: 4 March 2023
Accepted: 7 March 2023
Published: 9 March 2023

1. Introduction

The fast-changing communication technologies, such as the deployment of 5G and the development of 6G, greatly promote network bandwidth and data delivery quality for the mobile Internet, which effectively supports online services with high requirements of bandwidth and delivery performance (e.g., video-on-demand and video living) [1–4]. The video services rely on rich viewing content to attract a large number of users, which generates huge traffic demand and consumes a mass of network bandwidth [5–8]. Currently, there is a deep integration between video services and social networks. The video users make use of social links between them to distribute video resources, which opens up a new channel of video spread [9,10]. The frequent interaction and the close social relationships between users can speed up the diffusion process and promotes the diffusion scale. Increases in speed and scale of diffusion trigger a run on a bank for the bandwidth resources, which results in an overload of networks [11–15]. Different levels of network congestion caused by the violent squeezing of bandwidth resources bring long delays and high packet loss rate (PLR), which reduces the quality of experience (QoE) of users such as distortion or discontinuity of videos [16–19]. The high-efficiency allocation and utilization of network bandwidth based on the control of the diffusion process are significant for the scalability of video diffusion and the promotion of user QoE.

The social-based video diffusion is similar to an independent cascade: the carriers of video resources spread video data to their one-hop social neighbors [20–22]. Figure 1 shows the social-based video diffusion in wireless mobile networks. However, interest

preference for video content and social influence for neighbor partners play a decisive role in the progress and scale of the video diffusion process, which allows the diffusion process to be similar to the Epidemic model [23–25]. The users accept the propagative video data in terms of their interest preferences and their social influence affected by other users. The multiple diffusion process appears to be a discrete occurrence rather than a regularly stratified infection. The interest preference and social influence result in the chaotic spread, which increases the risk of a run on the bandwidth resources; on the other hand, not all users will accept the diffused video data because there are different conditions for the users to accept the pushed video data. The prediction of preference and influence effectively classifies users. The high-success push enables video content to pair users with appropriate interests and relationships, which achieves low-cost spread messages and well-organized diffusion. Moreover, the edge delivery of video data based on mobility awareness also effectively promotes the utilization efficiency of bandwidth resources and reduces variation levels of data transmission paths.

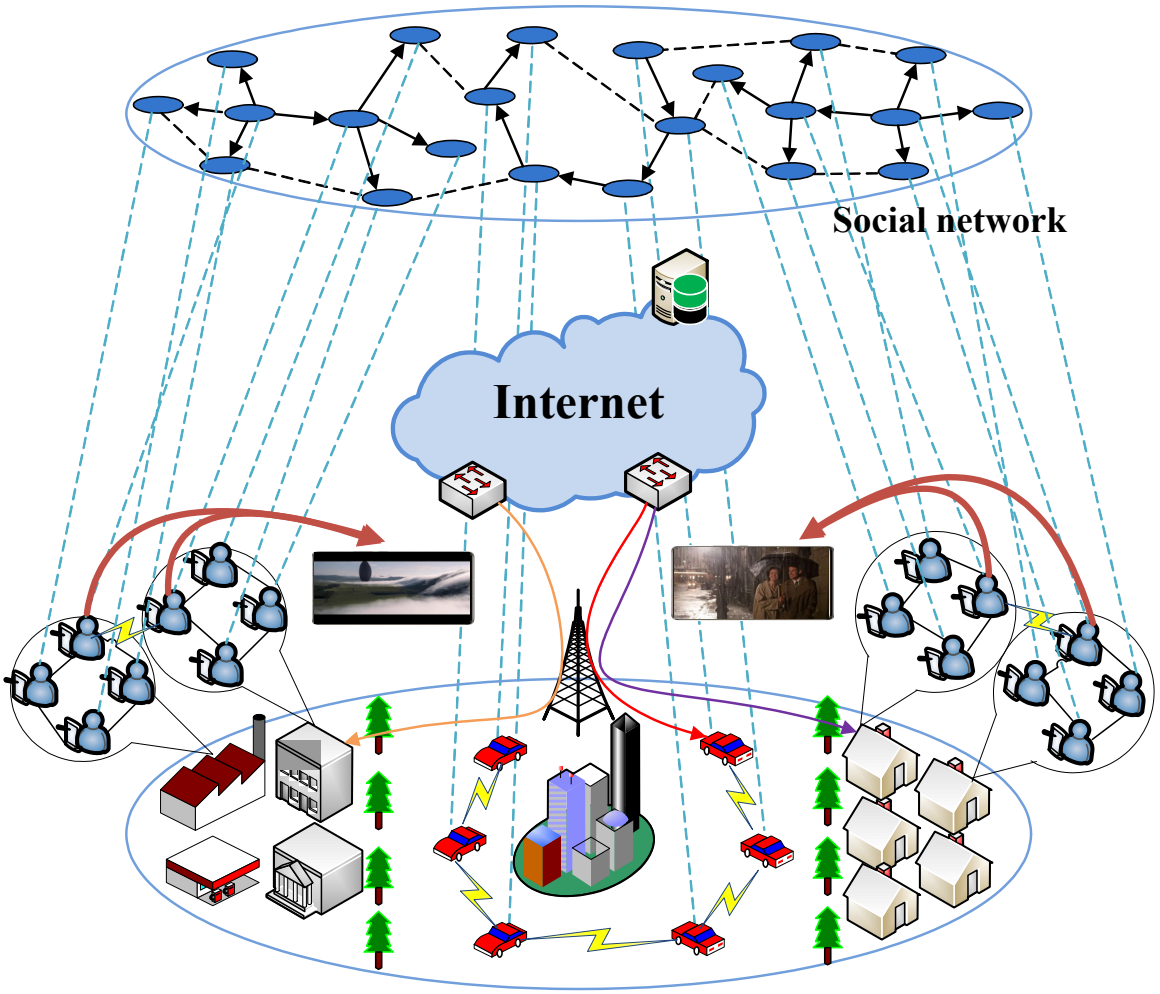

Figure 1. Social-based video diffusion in wireless mobile networks.

Recently, numerous researchers have paid close attention to the high-efficiency social-based video diffusion [26–28]. Some researchers focus on using social video-sharing methods to address the challenges of social video-sharing caused by boundless coverage and increased video content [29]. However, the above methods do not synthetically consider user interests and social influence to promote scale and efficiency of video propagation with effective launching. Some researchers also focus on social video propagation with the assistance of key nodes in social networks [30]. However, the above methods do not synthetically estimate the diffusion capacities of selected key nodes according to

user interests and social influence, so the accuracy levels of video launching are low. The existing social-based diffusion methods do not consider both interest preference and social influence, which does not ensure effective video launching with low message cost. Further, the mobility of mobile users is neglected by most methods, so the easy delivery of video data is subjected to dynamic transmission paths. The efficient video diffusion which implements effective launching in terms of interest and influence levels to promote diffusion scale with bandwidth-efficient data delivery based on awareness of mobility should be considered.

In this paper, we propose a Novel Epidemic-based Video Diffusion strategy using awareness of Sociality and Mobility in wireless networks (EVDSM). EVDSM formulates the measurement methods of interest preference and social influence of users and uses the measurement results to define the user roles in the Epidemic-based video spread process. EVDSM investigates the expected time length of data transmission and stability level of path structure to estimate the mobility levels of users. In the designed control strategy of video diffusion, EVDSM calculates the joint optimization results of pairing success rate and delivery performance according to user roles and mobility stability to formulate the priority levels pairing between infectors and candidate infectors, which achieves controllable video spread with efficient video sharing and high user QoE. Simulation results show how EVDSM achieves much better performance results in comparison with other state-of-the-art solutions. The main contribution of our work is introduced, as follows.

(1) EVDSM refers to participant roles and the propagation process of the Epidemic model to build a model of video diffusion which synthetically considers interest preference, social influence, and user mobility. EVDSM designs a measurement method of user interest levels for video content by joint consideration of content-based similarity between watched and popular videos and discrimination between user preference and popular videos. The weight value of social edges and the success rate of video push between users and the influence levels of neighbor nodes are used to estimate the social influence levels of users. Further, the expected time length of data transmission and the stability level of path structure is used to estimate user mobility levels;

(2) EVDSM defines user roles according to the four roles of the Epidemic model. EVDSM defines an estimation method of user roles according to interest preference and social influence and designs an identification method of user roles in terms of video-sharing behaviors of users. The users are labeled with the corresponding roles to support the role-based controllable video spread;

(3) EVDSM designs a control strategy of video diffusion with the consideration of video sharing performance and user QoE. The estimation results of joint optimization of pairing success rate and video delivery performance according to user roles and mobility stability are used to define the priority levels of pairing between infectors and candidate infectors. The control of video spread can promote the effectiveness of video sharing and ensure user QoE.

2. Related Work

Some researchers continuously focus on social-based video-sharing methods. Chiang et al. propose a novel collaborative social-aware QoE-driven video caching and adaption framework (CSQCA) [29]. CSQCA designs a collaborative video caching architecture based on two-layer multi-access edge computing. The popular videos are cached in multiple edge servers. CSQCA designs a social-aware proactive cache strategy by investigating user interactions and a social-based video dissemination process. CSQCA designs a QoE-driven video adaptation algorithm, which dynamically transcodes the cached videos to meet the various request. Zhang et al. propose a collaboration mechanism between IoVT devices with social attributes [31]. The IoVT devices construct the D2D collaborative group where video content is shared among intragroup members via D2D links, which effectively offloads controlled traffic of IoVT devices and video data. A collaborative video streaming strategy is designed based integration of flexibility of D2D communications

and scalable-high-efficiency-video-coding streams, which reduces the negative influence of network instability. Hsu et al. propose a social-aware P2P video transmission strategy for multimedia IoT devices [32]. Multimedia IoT devices are grouped as a peer-to-peer (P2P) network and implement communications and interactions with each other in the P2P network. Users classify social neighbors as having different priority levels in terms of social relationships. The social relationships, transmission progresses of video data, and mutual resource-sharing contributions of users are estimated and used to construct the weighted queuing priority classes of users. The users are added to the weighted fair queue in sequence according to the weighted queuing priority classes. The users with high-priority classes are selected as the suppliers to transmit video data for the video requesters, which reduces the negative influence levels of free riders and high QoE via multimedia IoT devices. Langa et al. propose a novel and lightweight social VR platform to achieve an interactive live TV show via a professional piece of VR content [33]. Realistic volumetric representations and affordable capturing systems are designed, which integrate remote users in shared virtual environments in real-time without the use of synthetic avatars. The heterogeneous media formats such as 3D scenarios, dynamic volumetric representation of users, and (live/stored) stereoscopic 2D and 180/360 videos also are integrated. The interaction between volumetric users and a video-based presenter with low delay supports dynamic control of the media playout. Cao et al. propose a social-aware D2D-based video multicast system by investigation of cooperation between mobile users to implement cooperative video multicast and allocate D2D radio resources [34]. By constructing a model of cooperation among mobile users in terms of social trust and social reciprocity, the users are grouped into multiple clusters to obtain the lost frames with the help of compensated frames of other users, which promotes user quality of experience. A video resource allocation scheme was designed to handle video requests of D2D radio of intragroup users.

Some researchers continuously focus on social-based video delivery methods. Hu et al. propose a social video replication and user request dispatching mechanism in the cloud content delivery network architecture [35], which reduces the maintenance cost of video systems and delivery delay of video data. The users are clustered into multiple communities in terms of social relationships, geographical location, and interest preference. A community-based strategy of video replication and request dispatching is designed and formulated as a constrained optimization problem. By making use of a stochastic optimization framework, the formulated constrained optimization problem was proved. Fan et al. propose a delivery prediction method of social-aware video content by employing the combined delivery prediction of video content [36]. A prediction problem of probability that a video is requested for efficient video content delivery in mobile social networks is formulated. A social- and content-aware video content delivery prediction method is designed in terms of the active degree of users, the similarity between videos, video popularity, interest preference, and social relationship. Zhang et al. propose a social-aware D2D video delivery method in a 5G ultra-dense network by measurement of mobility similarity [37]. By construction of a social state transition model of user movement based on encounter duration and shared video length to describe state transition conditions, a clustering algorithm of encounter events is proposed in terms of similarity between encounter events, so that the patterns of encounter events with common characteristics are extracted. The clustered encounter events are further refined and are extracted patterns of encounter events. Based on the extracted counter patterns, a sample-efficiency rapid recognition algorithm of encounter pattern is designed, which achieves fast heuristic recognition of encounter pattern and supports encounter-based video delivery with D2D communications. Wang et al. review the challenges, approaches, and directions of social-aware video delivery [38]. The challenges in social-aware video delivery are present according to the increasing data volume of user-generated video content and the boundless coverage of socialized sharing. A principal framework for social-aware video delivery is designed. The unique characteristics of social-aware video access and social content

propagation are analyzed and formulated. Kilanioti proposes a multimedia content delivery method in social networks [39]. By making use of user activity in social networks to stimulate multimedia content prefetching, a dynamic strategy of multimedia information transmission is designed, which reduces network bandwidth load and the maintenance cost of surrogate servers. Rajapaksha et al. propose a video content delivery method in social-based CDNs to reduce the overall network energy consumption [40]. The CDNs and P2P networks are combined by social connections between users to reduce the number and delay of data forwarding where users directly share video content via social connections. Users maintain stored videos in local buffers and supply video data for other users via P2P connections.

Some researchers continuously focus on social-based video diffusion methods. Niu et al. constructed a multi-source-driven asynchronous video diffusion model in social networks [41]. By investigation of the latency of information propagation along social links, the single-source activation latency of users in social networks was defined and follows the exponential mixture model. The temporal factor and the influence of multiple sources were incorporated, which can describe the propagation process of influence. The conclusion that activation probabilities of users exponentially decrease with increasing time is revealed. Moreover, the scale of active users who are close to source users determines the time variation of the exponential function and the influence levels of active users determine the total activation probability. By making use of maximum likelihood techniques, the algorithm of the parameter learning method of expectation maximization is designed. Long et al. construct a model of video viewing and sharing behaviors in social networks [42]. By a collection of viewing and sharing statistics of videos in a social video application, the temporal dynamics of video viewing and sharing behaviors during the diffusion process are obtained, which can handle the external influence and periodicity properly. Jiao et al. propose a video diffusion method by clustering users and selecting the specified relay nodes in clusters to cooperatively distribute videos [43]. The nodes are grouped into multiple clusters according to social influence and interest preference. The cluster head nodes are selected according to social influence and interest preference and act as the relay nodes to achieve cooperative distribution. A video distribution method based on the assistance of relay nodes is designed, which achieves mobility-aware cooperative video sharing based on collaboration between edge nodes. Hu et al. construct an indirect game model for the interaction reciprocity between users [44]. The Markov decision process is used to describe the decisions of users to maximize cooperation levels. Wu et al. propose a D2D-based cooperative video-sharing method based on cooperation in video caching and sharing between users [45]. The allocation of appropriate video providers for video requesters relies on investigating historical watched records, sharing initiative, geographical location, and QoE requirements. Selecting right video providers can effectively promote lookup success probability and data delivery performance. However, the above methods also do not synthetically estimate the propagation capacities of selected key nodes according to user interests and social influence, so the accuracy levels of video launching are low.

3. EVPSM Overview

Figure 2 illustrates the design of EVDSM architecture consisted of the measurement of interest levels of nodes, measurement of user roles, measurement of node mobility, and control strategy of video diffusion.

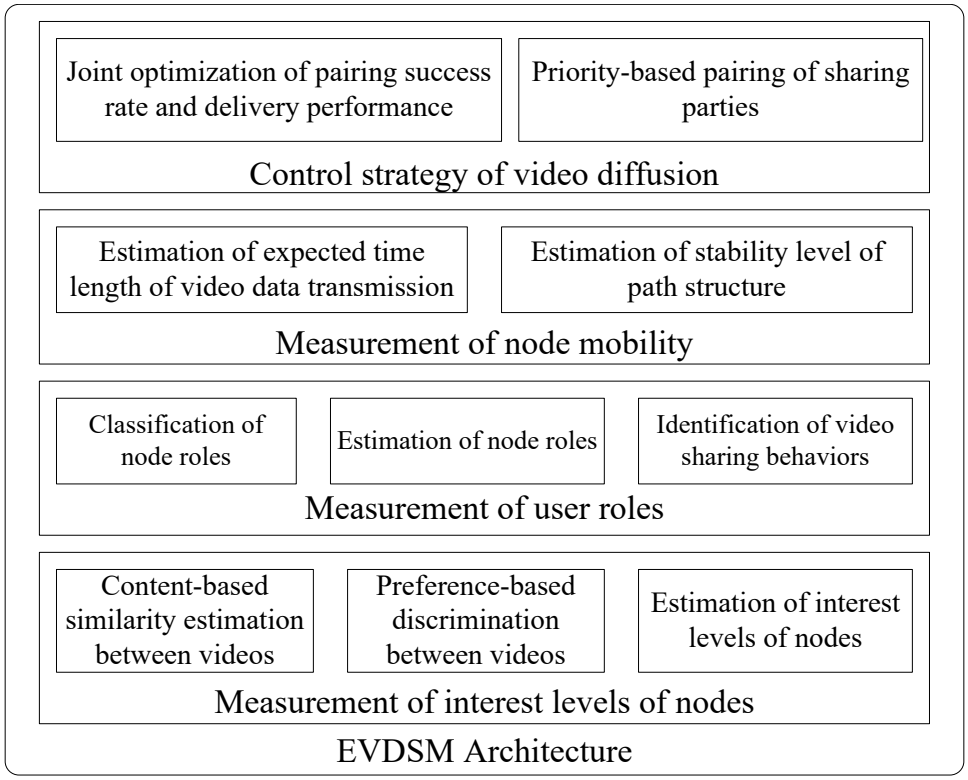

Figure 2. EVDSM architecture.

(1) Measurement of interest levels of nodes: The estimation of content-based similarity between popular videos and historical videos watched by nodes can show the interest levels of nodes for current popular videos; Estimating preference-based discrimination also reflects different levels between popular videos and historical videos watched by nodes; Estimating interest levels can effectively measure probabilities that nodes accept the popular videos in terms of joint similarity and difference between popular videos and historical videos watched by nodes;

(2) Measurement of user roles: The classification of node roles relies on epidemic-based four roles by investigating interest preference and social influence; The estimation of node roles formulates membership rules of node roles; The identification of video sharing behaviors makes use of the membership rules of node roles to recognize roles of nodes to pair parties of video sharing. The measurement of user roles can define recurrent behaviors of nodes and classify nodes in terms of distinguished roles;

(3) Measurement of node mobility: The estimation of the expected time length of video data transmission shows the communication quality of transmission paths of video data. Estimating the stability level of path structure shows the negative influence levels of node mobility for the communication quality of paths. The measurement of node mobility jointly considers data transmission performance and path structure stability, which promote measurement accuracy of node mobility variation;

(4) Control strategy of video diffusion: The joint optimization of pairing success rate and delivery performance can balance sharing scale and user QoE. The priority-based pairing of sharing parties can control the scale of video diffusion by selecting paired parties at the joint optimization of pairing success rate and delivery performance, which ensures the delivery performance of video data.

4. EVPSM Detailed Design

The social networks can be defined as a graph, $G = (V, E)$. V is the set of vertexes in G. Each user is a vertex in G. E is the set of edges in G. The two vertexes construct an edge when they communicate with each other. The users use the edges between them

in G to share video data. The push is the main way of video diffusion in G. The users who store video data also push video data to other users along the edges in G, which extends the range of video distribution and increases the scale of upload bandwidth of video data supply. A large amount of network bandwidth is consumed by the interactive messages and delivered video data in the process of video diffusion, which causes network congestion. The bandwidth-efficient video diffusion becomes the key way to reduce the contradiction between the supply and demand of network bandwidth.

To reduce the message scale of video push, the probability that the users accept the video data should be pre-estimated before pushing video data, which decreases the invalid messages of video push. User interests in the video content and the social relationship between pushers and accepters are crucial factors for a successful video push. User interests are the relatively stable property of users by long-term accumulation for various video content and are one of the decisive factors for acceptance of video data. Estimating user interests in the pushed videos according to user preference is important for video diffusion with a high success rate. On the other hand, there is a complex social relationship between video users (e.g., relatives, colleagues, and friends). The lasting social relationship not only can support the video users to keep continuous communications between them but also enables social networks consisting of video users to keep relatively static. Stable social networks with low-cost maintenance boost the spread of video resources because video users make use of social relationships to share video resources. Therefore, estimating the social closeness levels between users also is another important factor for video diffusion with a high success rate.

However, the social relationship only is a channel of video diffusion, which cannot ensure high-efficiency diffusion using social links between users. To reduce bandwidth waste in the process of video data transmission, near-end delivery of video data (e.g., one-hop transmission) should be ensured. The users use the intelligent handheld terminal to fetch and watch video content. The dynamic geographical location between suppliers and requesters of video data causes variations in the data transmission path, which leads to bandwidth waste of relay nodes in the path of data transmission and the jitter of delay and packet loss. The video data delivery with low hop and stable paths of data transmission is a crucial factor for the high-efficiency utilization of network bandwidth.

The process of video diffusion in G seems to be a cascade from vertex to vertex. However, the influence of content interests and social relationship enables the diffusion process to follow the epidemic model: the users who store video data are considered the infectors. The users who lose their interests are considered the immune users; the users who have interests are considered the susceptibles. When the users who store video data do not copy the data to other users and lose their interest or complete the task of video diffusion, the diffusion process in the epidemic model reaches an end state.

4.1. Measurement of User Interest Level

User interest in video content is the intrinsic factor that primarily determines the results of acceptance and rejection of the pushed videos. The long-term and stable interests in a kind of video with similar content form a clear preference. The users have a clear preference for video content such as a taste for comedy and resistance to tragedy. The pushed videos which belong to the user preference may be accepted with high probability. The playback time of the pushed videos also keeps a high level relative to other videos with low-level interests, which can increase the time that the users storing video data provide services of data delivery for other users. However, the users do not always keep a high-level interest to watch video content when the videos have high similar content and low discrimination. The similar or repeated storyline also leads to the tiredness of users. Content immunity brings a negative influence on the probability of successful acceptance of videos and the length of playback time of videos. Measurement of the interest level of a user u_h for a new video v_i needs to jointly consider similarity and discrimination between v_i and videos watched by u_h.

Let $VC = (vc_a, vc_b, ..., vc_m)$ be a set of video categories and $v_i \in vc_k$. Let $\overrightarrow{a_i}$ be the vector quantity of a video v_i. $\overrightarrow{a_i}$ includes multiple attributions such as name, director, actors, and introduction of v_i. The content-based similarity between videos is calculated using the cosine of the angle between vectors. The similarity value of the two videos v_i and v_j can see the formula (1).

$$S(v_i, v_j) = \frac{\overrightarrow{a_i} \cdot \overrightarrow{a_j}}{||a_i|| \cdot ||a_j||}, S(v_i, v_j) \in [0, 1]. \tag{1}$$

vc_{hk} is a video set. Videos in vc_{hk} have been watched by u_h. $vc_{hk} \in vc_k$ and $v_i \in vc_{hk}$. The mean value of similarity between v_i and all items in vc_{hk} can see the formula (2).

$$\overline{S_{ihk}} = \frac{\sum_{c=1}^{|vc_{hk}|} S(v_i, v_c)}{|vc_{hk}|}. \tag{2}$$

$|vc_{hk}|$ returns the number of all items in vc_{hk}. $\overline{S_{ik}} \in [0, 1]$ denotes the similarity level (degree of membership) between v_i and vc_{hk}. The larger the value of $\overline{S_{ihk}}$ is, the higher the degree of membership between v_i and vc_{hk} is. According to similarity between v_i and each item in vc_{hk}, the discrimination between v_i and vc_{hk} and can see the formula (3).

$$D_{ihk} = \frac{\sum_{c=1}^{|vc_{hk}|} \frac{\overline{l_c}}{L_c} |S(v_i, v_c) - \overline{S_{ihk}}|}{|vc_{hk}|}. \tag{3}$$

$S(v_i, v_c) - \overline{S_{ihk}}$ denotes the deviation between the similarity of v_i and v_c and average similarity of v_i and all items in vc_{hk}. The larger the value of $S(v_i, v_c) - \overline{S_{ihk}}$ is, the higher the discrimination level between similarity of v_i and v_c and similarity of v_i and all items in vc_{hk}. $\overline{l_c}$ is average playback time of v_c, L_c is the time length of v_c and $\overline{l_c} \in L_c$. $\frac{\overline{l_c}}{L_c}$ is the weight value of discrimination between v_i and v_c. This is as the playback time of the video is an important factor for the investigation of user interest level. If a user gives a lot of time to videos with high similarities, the user may have a high immunity level for the subsequent similar videos. D_{ihk} is the average value of weighted discrimination between v_i and each item in vc_{hk} and is considered as the interest offset of v_i relative to vc_{hk}. Moreover, because $|S(v_i, v_c) - \overline{S_{ihk}}| \in [0, 1]$ and $\frac{\overline{l_c}}{L_c} \in [0, 1]$, $D_{ihk} \in [0, 1]$.

The similarity of v_i and vc_{hk} denotes the membership level between v_i and vc_{hk}; Discrimination of v_i and each item in vc_{hk} denotes immunity level v_i and each item in vc_{hk}. A user has a high-interest level for a video v_i, v_i has high membership for a preferential video category of the user and has a clear distinction with each item in the preferential video category. Therefore, the interest level of u_h for v_i should be a result of a tradeoff between similarity and discrimination and can see the formula (4).

$$IL_{hi} = \alpha \times \overline{S_{ihk}} + (1 - \alpha) \times (1 - D_{ihk}), \alpha \in [0, 1]. \tag{4}$$

α is a regulatory factor and is used to achieve the optimization of similarity and discrimination. Because $D_{ihk} \in [0, 1]$ and $\overline{S_{ihk}} \in [0, 1]$, $IL_{hi} \in [0, 1]$. IL_{hi} represents the interest level of u_h for v_i.

4.2. Measurement of User Role

The users may play various roles in different diffusion contexts in terms of the diffusion process from person to person of the epidemic model, such as source users, followers, susceptibles, and immune users. For instance, the source users which have initial video data always undertake tasks of pushing and delivering video data for other users in the whole process of video diffusion, which can be considered as the infected users. The followers accept video data from the pushers with high probability and assist the pushers

to diffuse video data for a long time. The followers decide to accept video data in terms of property or pushers of video with a very high probability. The immune users are uninterested in the pushed videos and do not act any role in the process of video diffusion, which means that the immune users are not influenced by other users or video content for acceptance of videos. Unlike the immune users, the susceptible users have strong uncertainty for acceptance of videos and can be influenced by other users or video content.

The object selection of video push based on the priority estimation of video content and social factors is the key factor for high-efficiency video diffusion. For instance, the push messages of video data are sent to the infected users. The immune users do not need the overmuch push messages because of the low-level interest in the pushed videos. The followers only need one or a very small number of messages because of the high-level interests for the pushed videos or the close social relationship with the pushers. The susceptible users are subjected to the influence of video interests and social relationships to make the decision of acceptance and rejection for the pushed video data in terms of their preference and quit at any time for the video diffusion. More messages are used to address the problem of indeterminacy of susceptible users to increase the range of video diffusion.

The identification of user roles can effectively pre-estimate the function of users in the process of video diffusion, which reduces message overhead and the time cost of video diffusion. For instance, the followers and the immune accept and reject the pushed video data with a high probability. The susceptible users become the key factor for the efficiency and scale of video diffusion. Because the source users usually are marked, the source users are considered as the initial infected users. The identification of followers relies on the estimation of interest or social relationships. If a user u_h frequently accepts the videos pushed by the users with a close social relationship, u_h can be considered as the social follower; If u_h frequently accepts the videos with high-level interests, u_h can be considered as the interest follower. The common acceptance behaviors between u_h and other users for the same videos are the main measurement factor, which means that the main reason for acceptance of videos is the social relationship instead of interests. The acceptance success rate of a user u_h corresponding to another user u_k can see the formula (5).

$$FL_{hk} = \frac{|vs_h^k|}{|vs_{k\to h}|}, vs_h^k \in vs_{k\to h}. \tag{5}$$

vs_h^k is a set of videos which are pushed by u_k and are accepted by u_h; $vs_{k\to h}$ is of videos which are pushed by u_k. Each user is a collaborator in social-based video diffusion and receives multiple videos pushed by multiple users. The event that u_h accepts the only video pushed by u_k does not happen, namely $FL_{hk} = 1, vs_h^k = vs_{k\to h} = 1$ happens with a low probability. The average success rate of acceptance of u_h can see the formula (6).

$$\overline{FL_{ah}} = \frac{N_{ah}}{N_{ph}}, N_{ah} \in [0, N_{ph}]. \tag{6}$$

N_{ah} is the number that u_h successfully accepts the pushed videos; N_{ph} is the total number that u_h receives the pushed videos. $FL_{hk} - \overline{FL_{ah}}$ is the offset of following level of u_h relative to u_k and is in the range [−1,1]. The larger the value of $FL_{hk} - \overline{FL_{ah}}$ is, the closer the social relationship between u_h and u_k is. Let $\overline{FLO_k}$ be the average offset of the following level of all users in the whole social networks corresponding to u_k and see the formula (7).

$$\overline{FLO_k} = \frac{\sum_{c=1}^{|V|} FL_{ck} - \overline{FL_{ac}}}{|V|}. \tag{7}$$

V is the set of users in G and $|V|$ returns the number of items in V. $FL_{ck} - \overline{FL_{ac}}$ is the offset between u_k and each user u_c in social networks. Because $\overline{FL_{ah}} \in [-1, 1]$, $\overline{FLO_k} \in [-1, 1]$. $FL_{hk} - \overline{FL_{ah}} > \overline{FLO_k}$ denotes that u_h has the closer social relationship than

relationship between u_k and other users in social networks. u_h has a higher probability of accepting the videos pushed by u_k and can be considered as a social follower of u_k. If u_h is the social follower of a user u_k, we make the prediction that u_h necessarily accepts the videos pushed by u_k. Similarly, let N_{ahk} and N_{phk} be the number of accepted and pushed videos of u_h for the video category vc_k. The interest level of u_h for vc_k can see the formula (8).

$$ILC_{hk} = \frac{N_{ahk}}{N_{phk}}. \tag{8}$$

The average interest level of u_h for all video categories can see the formula (9).

$$\overline{ILC_h} = \frac{\sum_{i=1}^{|VC|} ILC_i}{|VC|}. \tag{9}$$

$ILC_{hk} - \overline{ILC_h}$ is the interest offset of u_h for vc_k, namely the interest level of u_h for vc_k relative to other video categories. The average interest offset of all users for vc_k in the whole social network can see the formula (10).

$$\overline{ILCO_k} = \frac{\sum_{c=1}^{|V|} ILC_{ck} - \overline{ILC_c}}{|V|}. \tag{10}$$

$\overline{ILCO_k}$ denotes the average interest level of all users for vc_k relative to other video categories. If $ILC_{hk} - \overline{ILC_h} > \overline{ILCO_k}$, u_h has the higher interest level for vc_k than that of the most of users and considered as the interest follower. Interested followers have a higher probability to accept the pushed videos than those of other video categories relative to other users in social networks. If u_h is the interest follower of a video category vc_k, we make the prediction that u_h necessarily accepts the videos which belong to vc_k. When a user is neither a source user nor a follower, they may be the immune users or the susceptible users. The interest levels are the main estimation factor for the identification of immune users. If $v_i \in vc_k$ is the pushed video to u_h, IL_{hi} is the interest level of u_h. Let VHS_h be the historical set of videos watched by u_h. The interest levels of all items in VHS_h can be calculated according to formula (4). The average interest levels of u_h for all items in VHS_h can see the formula (11).

$$\overline{IL_h} = \frac{\sum_{c=1}^{|VHS_h|} IL_{hc}}{|VHS_h|}. \tag{11}$$

If $IL_{hi} \leq \overline{IL_h}$, u_h is considered as the immune users; if $IL_{hi} > \overline{IL_h}$ and u_h is neither source user nor follower, u_h is considered as the susceptible users. The susceptible users do not have conspicuous following social and interested levels, but they have relatively high interest and relatively susceptible characters. The susceptible users have an uncertain probability of acceptance of the pushed videos, so the social relationship of other users and their interests in video content can influence the susceptible users to accept pushed videos. If a user u_p pushes a video $v_i \in vc_k$ to u_h, IL_{hi} and SI_{ph} denote interest level of u_h for v_i and social influence level of u_p. The probability that u_h accepts v_i pushed by u_p can see the formula (12).

$$P_{iph} = \beta \times IL_{hi} + (1 - \beta) \times SI_{ph}, \beta \in [0, 1], \tag{12}$$

where β is a regulatory factor for interest preference and social influence. The larger the value of P_{iph} is, the higher the probability that u_h accepts v_i pushed by u_p is. The value of SI_{ph} can be calculated according to the following equation.

$$SI_{ph} = w_{ph} \times R_{ph} \times \psi_h, \tag{13}$$

where w_{ph} is the weight value of edge between u_h and u_p in social networks and can see the formula (14).

$$w_{ph} = \frac{f_{ph}}{\sum_{c=1}^{|NS_h|} f_{ch}}, \tag{14}$$

where f_{ph} is the communications frequency between u_p and u_h; NS_h is the set of neighbor nodes of u_h in G and $|NS_h|$ returns the number of items in NS_h. w_{ph} denotes that the importance level of u_p relative to all neighbor nodes of u_h. R_{ph} the ratio of success rate of video push of u_p relative to all neighbor nodes of u_h and can see the formula (15).

$$R_{ph} = \frac{r_{ph}}{\sum_{c=1}^{|NS_h|} r_{ch}}, \tag{15}$$

where r_{ph} is the success rate of video push of u_p; The value of r_{ph} can see the formula (16).

$$r_{ph} = \frac{N_{sph}}{N_{tph}}, \tag{16}$$

where $N_{sph} \in [0, N_{tph}]$ is the number of successful pushing video of u_p for u_h; N_{tph} is the total number of video push of u_p for u_h. Because $r_{ph} \in [0,1]$, $R_{ph} \in [0,1]$. ψ_h is an influence factor of neighbor nodes of u_h for acceptance of v_i and can see the formula (17).

$$\psi_h = \frac{|NSS_h^i|}{|NS_h|}, \tag{17}$$

where $NSS_h^i \in NS_h$ is the subset of neighbor nodes which have accepted v_i of u_h and $|NSS_h^i|$ returns the number of items in NSS_h^i. ψ_h also denotes the influence level of social network environment of u_h for acceptance of v_i. The larger the value of ψ_h is, the higher the influence levels of the social network environment of u_h is. Because $w_{ph} \in [0,1]$, $R_{ph} \in [0,1]$ and $\psi_h \in [0,1]$, $SI_{ph} \in [0,1]$. Further, because $IL_{hi} \in [0,1]$ and $SI_{ph} \in [0,1]$, $P_{iph} \in [0,1]$. SI_{ph} is the important estimation factor for the pair between pushers and the pushed objects.

4.3. Measurement of User Mobility

Except for the high-success video push, the high-efficiency delivery of video data is also an important influence factor for the efficiency and performance of video diffusion. The length of data transmission paths between pushers and push objects determines the delivery performance of video data. The long paths include multiple relay nodes, so the bandwidth resources of relay nodes are wasted and the transmission delay is increased; On the other hand, the mobility of relay nodes also results in the variation of transmission paths, which increases the risk of packet loss and delay rise. The near geographical distance between pushers and accepters is an important indicator for transmission paths with low hop. For instance, if the geographical distance between pushers and accepters is less than M in wireless mobile networks, where M is the coverage range of one hop wireless signal, they use one-hop distance to implement high-efficiency transmission of video data because the transmission paths with one hop distance can directly deliver video data without the participation of relay nodes and obtain low delay and low probability of packet loss. The object selection of video push should consider critical reasons such as available bandwidth, packet loss, and path length.

The available bandwidth and packet loss are communication quality factors of transmission paths. The higher the available bandwidth of paths is, the shorter the transmission time of video data is. The low packet loss can decrease the retransmission number of video data, which reduces the transmission time of video data. Let $\overline{B_{hp}}$ be average band-

width of transmission path TP_{hp} between u_h and u_p during a time span from t_a to t_b. The transmission time of a video v_i can see the formula (18).

$$T_{ph}^{i} = \frac{size_i}{\overline{B_{hp}} \times (1 - PLR_{ph})}, \tag{18}$$

where $size_i$ is the size of v_i; PLR_{ph} is the average rate of packet loss of TP_{hp} during a time span from t_a to t_b. The lower the value of T_{ph}^{i} is, the better the communication quality and efficiency of TP_{hp} is. T_{ph}^{i} is a prediction value because the values of bandwidth and packet loss rate are the statistical-based mean values. Moreover, the length of TP_{hp} is the structure factor of transmission paths, which makes an impact on the communication quality and efficiency of TP_{hp}. If the length of TP_{hp} is long, TP_{hp} has many relay nodes. The mobility of relay nodes leads to the instability of TP_{hp} structure, which increases the risk of packet loss and delay rise. The bandwidth of relay nodes also is wasted for forwarding video data. The stability level of path structure of TP_{hp} can see the formula (19).

$$PS_{ph} = \frac{1}{\log_2(|RS_{ph}| + 1)} \times \frac{OT_{\min}^{ph}}{T_{ph}^{i}}, \tag{19}$$

where RS_{ph} is the set of all nodes in TP_{hp} and $|RS_{ph}|$ returns the number of items in RS_{ph}. $\log_2(|RS_{ph}| + 1) \in [1, +\infty]$ denotes the influence level of path length. The longer the path length of TP_{hp} is, the smaller the value of $\frac{1}{\log_2(|RS_{ph}|+1)}$ is. $OT_{\min}^{ph}$ is the minimum value among average duration time of one hop relationship between all adjacent nodes based on the geographical location in TP_{hp} where the range of value of $OT_{\min}^{ph}$ can see the formula (20).

$$OT_{\min}^{ph} = \begin{cases} OT_{\min}^{ph}, OT_{\min}^{ph} \in [0, T_{ph}^{i}) \\ T_{ph}^{i}, \quad OT_{\min}^{ph} \in [T_{ph}^{i}, +\infty). \end{cases} \tag{20}$$

The calculation of the average duration time of the one-hop relationship between all adjacent nodes based on the geographical location in TP_{hp} relies on the statistical information of duration time that the encountered nodes keep a one-hop relationship. $\frac{OT_{\min}^{ph}}{T_{ph}^{i}} \in [0, 1]$ denotes the stability level of path structure of TP_{hp} in the process of data transmission of v_i. $\frac{1}{\log_2(|RS_{ph}|+1)}$ is the weight value of $\frac{OT_{\min}^{ph}}{T_{ph}^{i}}$. The larger the value of path stability PS_{ph} is, the higher the efficiency of path TP_{hp} is. Because $\frac{1}{\log_2(|RS_{ph}|+1)} \in (0, 1]$ and $\frac{OT_{\min}^{ph}}{T_{ph}^{i}} \in [0, 1]$, $PS_{ph} \in [0, 1]$. According to the Equations (12) and (19), when u_p selects the objects of pushing v_i from the susceptible users, the priority level of a susceptible user u_h can see the formula (21).

$$\eta_{iph} = \beta \times P_{iph} + (1 - \beta) \times PS_{ph}, \beta \in [0, 1]. \tag{21}$$

Because $P_{iph}, PS_{ph} \in [0, 1]$, $\eta_{iph} \in [0, 1]$. The susceptible users are selected as the push objects by the infected users according to the priority estimation value η.

4.4. Control Strategy of Video Diffusion

The purpose of video diffusion focuses on extending the scale and range of distribution of video copies. The pointless waste and intensive bank runs of network bandwidth result in network congestion, so the high delay and packet loss caused by congestion results in a severe negative influence on user QoE. The video diffusion should take into account both diffusion regulation and high-utilization bandwidth. The diffusion regulation needs to set the order of diffusion in terms of pre-estimation results of the user role. For instance,

the users who are pre-estimated as followers can be activated via a video message and should have high priority. The users who are pre-estimated as immune users can be neglected, which saves the messages of pushing videos. Objects of pushing videos focus on the susceptible users which have high uncertainty for the acceptance and rejection of pushed videos. The initial source users discretely distribute in social networks and employ the cascaded spread way to diffuse v_i from one-hop social neighbors to multiple-hop social neighbors. In other words, an initial source user u_k firstly pushes v_i to social neighbors of u_k in G. After the social neighbors of u_k accept pushed v_i, they push v_i to their social neighbors. v_i is pushed to the whole social network via the cascaded spread.

The purpose of diffusion with low message cost requires that the initial source users effectively recognize the user role and preferentially distribute v_i to the followers in social neighbors and do not send the pushed v_i again for the immune users in social neighbors. Therefore, there are three steps for each user who has been infected in the process of the cascaded spread: (1) The infected users firstly push v_i for their social neighbors and receive the feedback information containing the results of role, η and PS; (2) The infected users optimally deliver data of v_i to the followers in terms of roles and PS; (3) The infected users also further deliver data of v_i to the susceptible users in terms of the received η. Let INS_i be the set of initial source nodes of v_i and INS_i also can be considered as a set of infected users; MNS_i is the immune users in G for the diffusion of v_i; Let x be the round of video diffusion in G. The control strategy of diffusion of a video v_i is described, as follows.

(1) Initially, x is set to 0 at the first diffusion round. INS_i is not an empty set and MNS_i, FNS_i and CNS_i are the empty sets.

(2) A user u_p is selected from all items in INS_i. Let SNS_p be the set of social neighbors of u_p. u_p removes the items in $INS_i \cap SNS_p$ and $MNS_i \cap SNS_p$ from SNS_p, which reduces the number of sent messages. u_p sends the information of v_i to all items in SNS_p. Every item in SNS_p returns a message containing estimation results of role, mobility, and acceptance probability. u_p records roles of social neighbors in SNS_p: u_p adds the neighbors which have stored v_i into a neighbor subset $SUS_P \in SNS_p$ and INS_i, respectively; u_p adds the immune neighbors into a neighbor subset $IUS_p \in SNS_p$; u_p adds the follower neighbors into a neighbor subset $FUS_p \in SNS_p$; u_p adds the susceptible neighbors into a neighbor subset $SUS_p \in SNS_p$.

(3) u_p preferentially delivers data of v_i to the follower neighbors. If FUS_p is an empty set, the current step is transferred to step 4. Otherwise, if FUS_p is not an empty set, u_p broadcasts a message containing information of all items in FUS_p to all items in INS_i. After all items in INS_i receives the message sent by u_p, they calculate the mobility values with all items in FUS_p and return the estimation results from PS to u_p. u_p allocates suppliers of v_i for every item in FUS_p. For instance, u_p selects an item u_e in FUS_p and implements the descending sort for the mobility results of all items in INS_i with u_e. The item u_d in INS_i, which has the maximum value of mobility with u_e, becomes a supplier of v_i corresponding to u_e. u_p sends a message containing information of u_d to u_e. If u_e agrees with the data delivery of u_d, u_e returns an acknowledgment message to u_p. After u_e sends a message containing information of u_e to u_d, the pair between u_e and u_d is finished. After the data delivery of v_i to u_e is finished, u_e is added into INS_i by u_d; The updated INS_i is broadcasted to each item in INS_i by u_d. Otherwise, if u_e rejects the data delivery of u_d, u_e is added into MNS_i by u_p. After u_e is added into INS_i or MNS_i, u_e removes u_e from FUS_p and broadcasts the updated INS_i or MNS_i to all items in INS_i, which enables the users in INS_i to avoid sending invalid messages. u_p iteratively pairs for other items in FUS_p in the same way.

(4) When u_p finishes the pair for all items in FUS_p, u_p further delivers data of v_i to the susceptible neighbors in SUS_p. If SUS_p is an empty set, the current step is transferred to step 5. Because the susceptible neighbors have strong uncertainty for acceptance of v_i unlike the follower neighbors, the diffusion of v_i for the susceptible neighbors in SUS_p employs the linear threshold method. For instance, u_f is a susceptible neighbor in SUS_p and has a social threshold ST_f. When u_f receives a video v_i pushed by u_p (u_f is a social neighbor of

u_p), the social influence cumulant for v_i can be updated according to the following formula:

$$ST_{fi}^{x} = ST_{fi}^{x-1} + \frac{cf_{pf}}{CF_f}, \tag{22}$$

where ST_{fi}^{x} is the social influence cumulant of u_f for v_i pushed by u_p at the x^{th} diffusion round and $ST_{fi}^{0} = 0$. $cf_{pf} \in [0, CF_f]$ is the interaction frequency between u_f and u_p in the process of video sharing; CF_f is the total interaction frequency between u_f and all social neighbors in the process of video sharing. If u_f accepts v_i pushed by u_p at the x^{th} diffusion round, u_f returns an acknowledgement message to u_p. u_p allocates an appropriate supplier for u_f refer to the above step 3; If u_f rejects v_i pushed by u_p at the x^{th} diffusion round, u_p receives a message returned by u_f where the message contains the updated ST_{fi}^{x} according to the formula (22). If $ST_{fi}^{x} \geq RT_s$ and u_f accepts v_i, u_p adds u_f into INS_i. If $ST_{fi}^{x} < RT_s$, u_p continues to push v_i to u_f at the $(x+1)^{th}$ round. Because each user has multiple social neighbors in G, u_f receives many messages containing the pushed v_i. u_f may have been add into INS_i or MNS_i at any given moment due to acceptance of v_i or $ST_{fi}^{x} \geq RT_s$. When u_p receives INS_i or MNS_i updated by other users and u_f has been added into INS_i or MNS_i, u_p removes u_f from SUS_p and does not push v_i at the $(x+1)^{th}$ round. u_p iteratively pairs for other items in SUS_p in the above same way.

(5) When the time of current x^{th} round is completely consumed, the current x^{th} round is in an end state. If FUS or SUS of all items in INS_i is not the empty set, the current implementation returns to step 2; Otherwise, if FUS and SUS of all items in INS_i are empty sets, the diffusion process of v_i is terminated.

The above diffusion process is described in Algorithm 1.

Algorithm 1: Control process of v_i diffusion.

x is round number of propagation of v_i and $x = 0$;
SNS is social neighbor set;
FUS is follower neighbor set;
SUS is susceptible neighbor set;
$F_i = 1$ is flag of diffusion termination;
while $F_i = 1$
for(c=0;c<$|INS_i|$;c++)
  if $x = 0$
    $SNS_h = SNS_h - INS_i \cap SNS_h$;
    $INS_i[h]$ broadcasts v_i to items in SNS_h;
    $INS_i[h]$ records information returned by items in SNS_h;
  else
    $SNS_h = SNS_h - INS_i \cap SNS_h - MNS_i \cap SNS_h$;
  end if
  $INS_i[h]$ broadcasts FUS_h to items in INS_i;
  $INS_i[h]$ records information returned by items in INS_i;
  for(c=0;c<$|FUS_h|$;c++)
    $INS_i[h]$ pairs $FUS_h[c]$ and items in INS_i;
    if $FUS_h[c]$ rejects pairing
      $FUS_h[c]$ is added into MNS_i;
    else $FUS_h[c]$ is added into INS_i;
  end for

Algorithm 1: *Cont.*

$INS_i[h]$ broadcasts v_i to items in SUS_h;
$INS_i[h]$ records information returned by items in SUS_h;
for(c=0;c<|SUS_h|;c++)
  if $ST_{ci}^{x} \geq RT_s$ and $SUS_h[c]$ accepts v_i
    $SUS_h[c]$ is added into INS_i;
  else if $SUS_h[c]$ rejects v_i
    $SUS_h[c]$ is added into MNS_i;
  end if
 end for
end for
if FUS and SUS of all items in INS_i are empty
 $F_i = 0$;
else x++;
end if
end while

5. Testing and Test Results Analysis

We compare the performance of the proposed solution EVDSM with that of the two state-of-the-art solutions DMSEM [37] and OCP [46] in a mobile network environment by making use of the Network Simulator 3 (NS-3). A square scenario with 3000 × 3000 m^2 area has 500 mobile nodes. The three solutions employ the random movement model of mobile nodes. The mobile nodes keep random movement behaviors during 500 s simulation time. Position coordinates of beginning and ending and movement speed of all mobile nodes are randomly allocated in advance at initial simulation time. The mobile nodes keep uniform motion along the path consisted of beginning and ending position coordinates using the allocated speed. When the mobile nodes arrive at the appointed ending position, they are allocated the new random destination position, and the movement speed, namely the stay time of mobile nodes is 0 s. The mobile nodes move to the new target position without a break using the new allocated speed. [1, 30] m/s is defined as the speed range of mobile nodes. The number of videos that are requested by mobile nodes is set to 40. The popularity of all videos follows the Zipf distribution [47]. The probability of requesting the n^{th} popular video see the formula (23) [48]:

$$P(n) = \frac{\sum_{40}^{i} i^{\rho}}{r^{\rho}}. \tag{23}$$

The process in which the mobile nodes request videos during the whole simulation time follows the Poisson distribution. Initially, the mobile nodes request videos in terms of the video request probabilities. At the moment, the mobile nodes are allocated random playback time. When the mobile nodes finish the playback according to the allocated playback time, they continue to request the new videos according to the request probabilities. The length and size of every video are 100 s, which means that the random playback time is in the range [1, 100] s. The size and playback bitrate of every video is 25 MB and 2000 kbps, respectively. The number of videos that are stored in the local buffer of mobile nodes is 10. Every mobile node can store 10 videos in the local buffer. The nodes which provide initial video data are defined as the source nodes. Every source node can store 10 different videos to provide supply services of video data for the request nodes, which means that 40 nodes provide the initial data of 40 videos. 20,000 log entries which are considered historical playback trace libraries are generated, which supports the measurement of social relationships and interest preference. The historical movement trace library is generated, which supports mobility estimation of EVDSM and encounter pattern extraction of DMSEM.

The simulation scenarios have 36 base stations which act as the access points (APs) to transmit and forward data. The settings of the physical and MAC layer and modulation

schemes of network units follow the 5G industrial standardization. The MAC protocol employs 802.11p and the upper bound of the data rate is set to 27 Mbps. The maximum communication range is 250 m; The MAC channel delay is 250 ms. The propagation loss model employs the Friis Propagation Loss Model (FPLM) in NS-3 [49] to eliminate the performance degraded by random shadowing effects for an unstructured clear path between receivers and transmitters. The FPLM effectively erases the random effects caused by shadowing for the simulation results. The D2D settings of the 5G network follow the settings in the popular studies [50].

Testing Topology and Scenarios

We compared the performance of EVDSM with DMSEM and OCP in terms of the startup delay (SD), average data transmission delay (ADTD), packet loss rate (PLR), average freeze time (AFT) and peak signal-to-noise ratio (PSNR), respectively.

Startup delay (SD): Let $t_{ri} - t_{si}$ be the startup delay of a requesting node n_i where t_{si} is time that n_i sends a request message to the video supply node n_j and t_{ri} is the time that n_i receives the first video data sent by n_j. The average SD values see the formula (24).

$$\overline{SD} = \frac{\sum_{i=1}^{n} SD_i}{n}. \tag{24}$$

n is the number of nodes which finish startup; SD_i is i^{th} startup delay. In Figure 3, $\overline{SD}$ denotes the average SD values every 5 s. As Figure 3 shows, the three curves corresponding to the three solutions corresponding to EVDSM with DMSEM and OCP have the process of slow fall after a fast rise with the fluctuation. The red curve of EVDSM first experiences a fast rise from t = 0 s to t = 190 s, has a stable rise from t = 200 s to t = 270 s, has a fast fall from t = 280 s to t = 400 s and has a slow fall from t = 410 s to t = 500 s. The orange curve of DMSEM has a fast rise from t = 0 s to t = 170 s, experiences a stable rise from t = 180 s to t = 270 s, experiences a fast fall from t = 280 s to t = 340 s and has a slow fall from t = 350 s to t = 500 s. The green curve of OCP has a fast rise from t = 0 s to t = 250 s and keeps a slow fall trend from t = 260 s to t = 500 s. The SD values of EVDSM are less than those of DMSEM and OCP during the most of simulation time. The peak value of the blue curve corresponding to EVDSM is less than those of DMSEM and OCP.

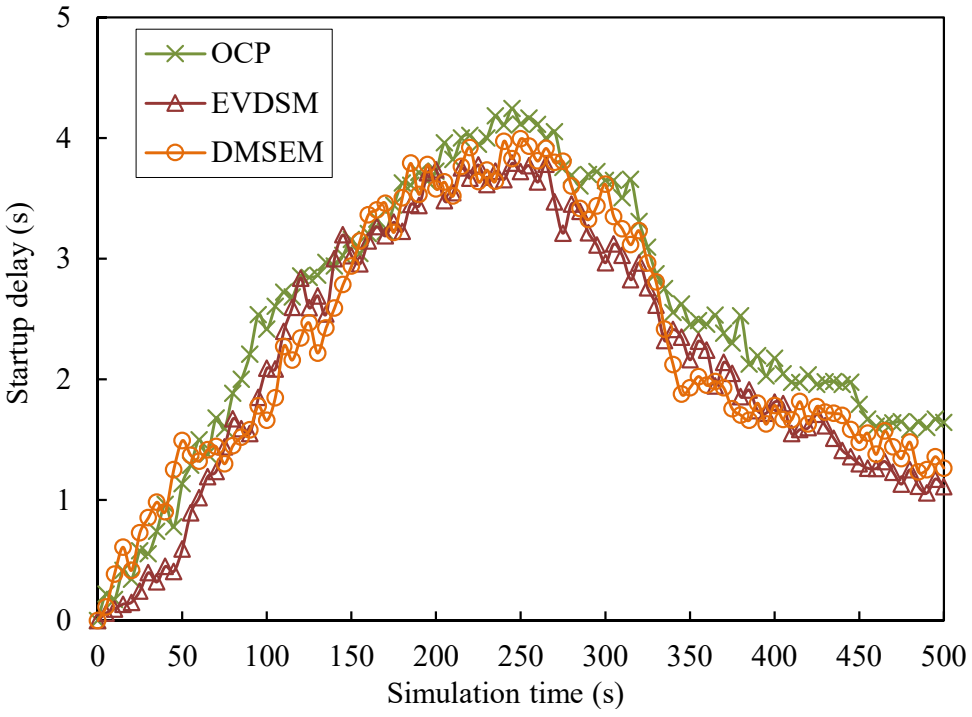

Figure 3. Startup delay against simulation time.

Figure 4 shows the average SD values corresponding to the three solutions with the different speed ranges of nodes. The average SD values have a rising trend with an increasing speed range of nodes. The red bars of EVDSM experience a slow rise from the range [1, 5] to [10, 15], have a fast rise from the range [10, 15] to [15, 20] and have a slow rise from the range [20, 25] to [25, 30]. The orange bars of DMSEM have a slow rise from the range [1, 5] to [10, 15] and have a uniform rise from the range [10, 15] to [25, 30]. The green bars of OCP keep the fast rise trend from the range [1, 5] to [10, 15] and experience a slow rise from the range [15, 20] to [25, 30]. The SD values of EVDSM are less than those of DMSEM and OCP.

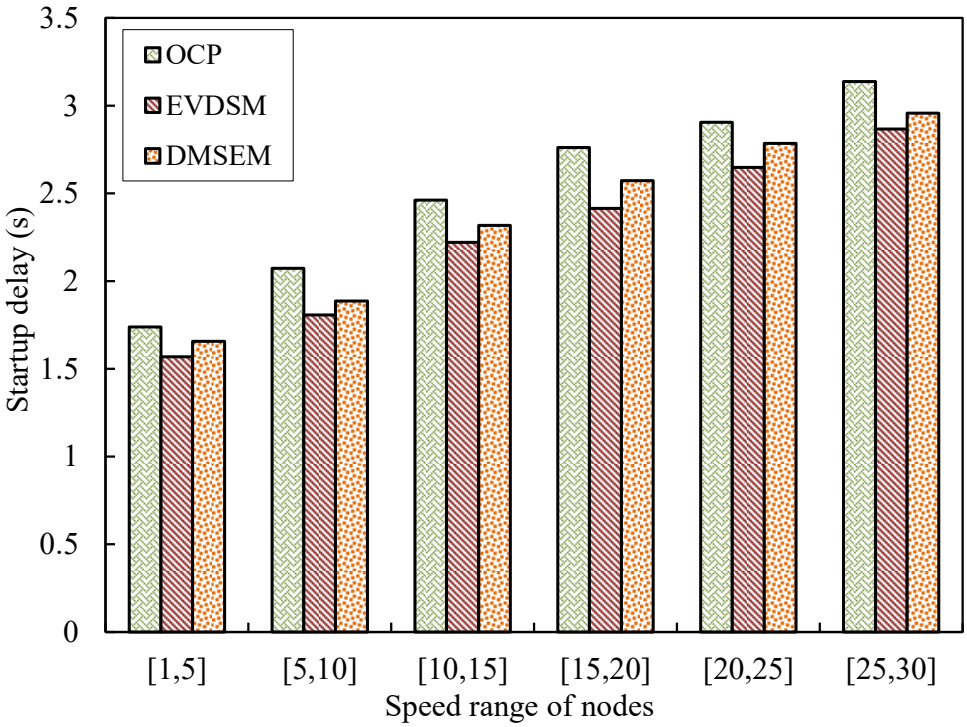

Figure 4. Startup delay against various speed ranges of nodes.

Initially, the small-scale requests do not bring a large load of video traffic, so the startup delay keeps the low levels. However, the dynamic watch time of users leads to repeated requests for diverse videos. Even if the successful video push also does not ensure long watch time and reduce the number of requests. The large-scale video requests for different videos promote a load of video supply so that the search time of video supply and the time of handling request messages are lengthened. Moreover, the increase in the mobility of nodes also promotes the probability of packet loss, which also increases startup delay. The decrease in the number of request nodes reduces the load of supply. The optimized video distribution effectively reduces the search time of video supply and the time of handling request messages. The values of startup delay fast decrease. EVDSM pairs the appropriate suppliers for potential video requesters with high probabilities of requesting videos at a proper time and allocates the suppliers with optimal delivery performance for video requesters by investigating interest preference, social influence, and user mobility. EVDSM refers to participant roles and the propagation process of the Epidemic model to estimate interest preference, social influence, and user mobility for an exact video push with high success probability and excellent delivery performance. By joint consideration of content-based similarity between watched and popular videos and discrimination between user preference and popular videos, EVDSM effectively estimates user interest levels for video content, which promotes success probabilities of video push and fast finds the appropriate supply nodes for the video request nodes. The successful video push reduces the lookup delay. EVDSM defines the estimation rule of user roles according to interest

preference and social influence and identifies user roles in terms of video sharing behaviors of users, which effectively defines the range of video sharing and reduces the number of useless pushes. EVDSM investigates the expected time length of data transmission and stability level of path structure in historical transmission traces of video data to estimate variation levels of user mobility, which reduces the negative influence caused by user mobility for video delivery performance. EVDSM makes use of priority-based pairing between video supply nodes and user mobility request nodes to effectively push videos. EVDSM makes use of role identification to predict the scale of video demand and relies on video push to promote the scale of video supply, which balances supply and demand with various demands. Therefore, the SD values of EVDSM are lower than those of DMSEM and OCP at the most of simulation time. DMSEM collects and clusters encounter of nodes to extract encounter patterns to predict encounter between mobile nodes in the future, which is used to pair D2D communication parties with one-hop geographical distance and supports video data delivery via one-hop D2D communications. DMSEM considers the influence caused by the mobility of nodes based on clustering encounter events that have similar encounter duration and variations of geographical distance. The long-term stability of the one-hop D2D communication path reduces interference of path variation to support high-efficiency video data transmission. The encounter-based data transmission lengthens the wait delay of transmission and forwarding of data. The random mobility of data also increases the risk of D2D communication interruption, which further increases the wait delay for the transmission and forwarding of data. On the other hand, the limited area and fast speed can promote probabilities of encounter of mobile nodes, so that DMSEM has the better performance of SD. In OCP, the nodes exchange state lists with each other to share information on video distribution to achieve dynamic regulation of video caching. OCP makes use of the collected distribution information to predict the demand variation of the whole system, which increases and adjusts the video distribution of the whole network in advance to provide enough video supply. All nodes follow the caching decision to implement caching and replacement of videos at a uniform period, which effectively addresses the problems of scale and allocation of video supply caused by large-scale video demand. The fast variation of demand brings a great challenge for the timeliness of caching and replacement of OCP. Moreover, OCP does not consider the influence of node mobility on data delivery. Therefore, the SD values of OCP slightly is larger than those of EVDSM and DMSEM.

Average data transmission delay (ADTD): The average data transmission delay see the formula (25).

$$ADTD = \frac{\sum_{i=1}^{n} dt_i}{n}. \tag{25}$$

n is the number of transmission delays of video data during a period t and dt is transmission delay of video data. The ADTD values every 5 s are shown in Figure 5. As Figure 5 shows, the three curves corresponding to EVDSM with DMSEM and OCP have a severe jitter process with the increasing simulation time and keep a fall after a rise. The ADTD values of EVDSM have lower levels than those of DMSEM and OCP and the ADTD peak value of EVDSM is less than those of DMSEM and OCP. The ADTD peak value of DMSEM is lower than that of OCP.

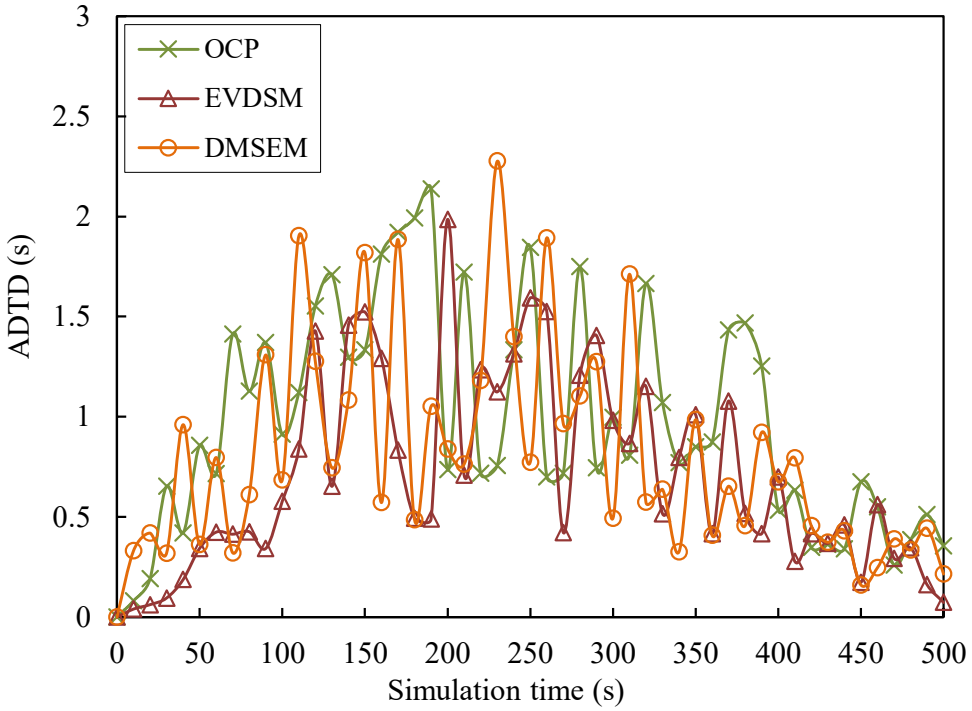

Figure 5. Average data transmission delay against simulation time.

As Figure 6 shows, the average ADTD values corresponding to the three solutions have a trend of slow rise with an increasing speed range of nodes. The red bars of EVDSM keep the slow rise trend from the range [1, 5] to [10, 15] and have a fast increase from the range [15, 20] to [25, 30]. The orange bars of DMSEM have a slow rise from the range [1, 5] to [10, 15] and a fast rise from the range [15, 20] to [25, 30]. The green bars of OCP keep the fast rise at all ranges of video speed. The red bars of EVDSM are lower than those of DMSEM and SECS.

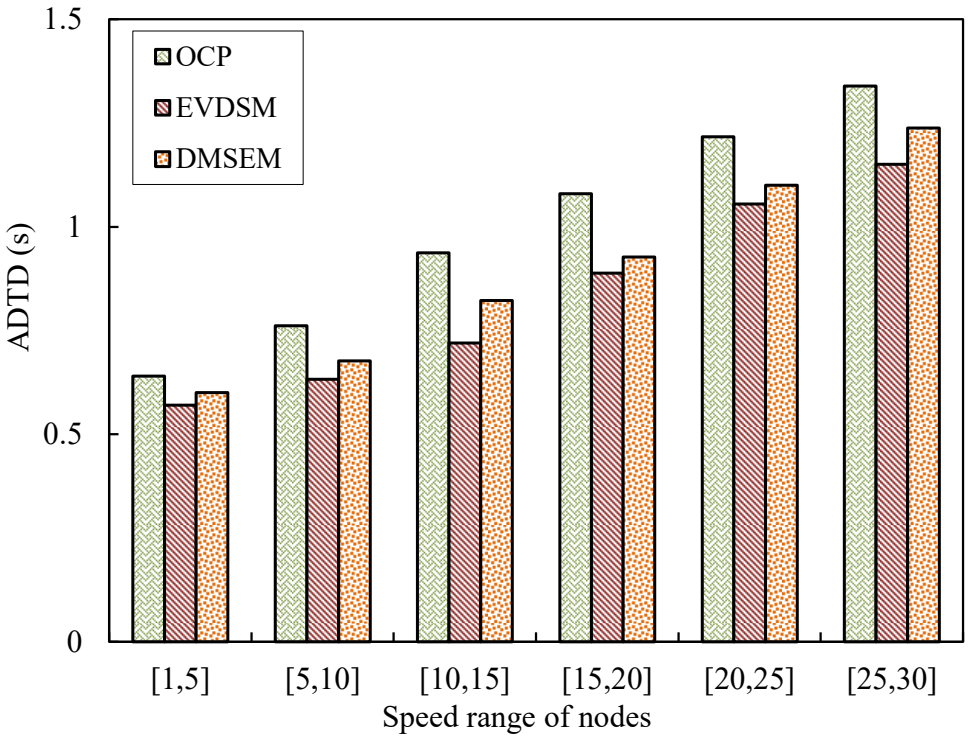

Figure 6. Average data transmission delay against various speed ranges of nodes.

EVDSM estimates variation levels of node mobility by investigating the expected time length of data transmission and stability level of path structure based on the analysis of historical transmission traces of video data. EVDSM makes use of available bandwidth and packet loss to estimate the performance of data transmission; EVDSM relies on the duration time of one hop relationship between all adjacent nodes based on the geographical location to estimate structure stability levels of the data transmission path. Therefore, EVDSM can ensure high performance of data transmission. However, the mobility of nodes brings a severely negative influence on the transmission performance of video data. The ADTD values of EVDSM also fast increase with the increasing speed of node movement speed, so the SD values of EVDSM are slightly lower than those of DMSEM and OCP. DMSEM depends on encounter-based D2D communications to implement video data delivery. To reduce the negative influence caused by node mobility, DMSEM collects and analyzes encounters of nodes and clusters encounter events that have similar encounter duration and variation of geographical distance, which effectively classifies encounter events to support data transmission with different requirements of data transmission time. DMSEM further extracts the encounter patterns from the encounter clusters to recognize and predict encounter events. DMSEM can rely on encounter-based D2D communications to support high-efficiency data transmission. However, node mobility is the main influence factor for D2D communications. The fast movement of nodes leads to the interruption of D2D communications, which greatly increases the transmission delay of data. Therefore, the ADTD values of DMSEM keep a fast rise trend with increased movement speed. Because OCP does not consider the influence of node mobility for data delivery and neglects the measurement of data transmission performance, the ADTD values of OCP are larger than those of EVDSM and DMSEM.

Packet loss rate (PLR): The ratio between the number of lost video data during a period t and the total number of sent video data during t is defined as the packet loss rate.

The PLR values during the period t = 10 s are shown in Figure 7. As Figure 7 shows, the three solutions keep the fall trend with a slight fluctuation during the whole simulation time. The red curve of EVDSM has a fast fall trend from t = 0 s to t = 200 s and keeps a slight decrease with the slight fluctuation from t = 210 s to t = 500 s. The PLR curve of EVDSM is lower than those of DMSEM and OCP during most of the simulation time. The orange curve of DMSEM has a fast fall from t = 0 s to t = 140 s and a slow fall from t = 150 s to t = 270 s and keeps a stable trend from t = 280 s to t = 500 s. The green curve of OCP has a fast fall from t = 0 s to t = 140 s, experiences a slight fall from t = 150 s to t = 360 s and keeps a stable decrease from t = 370 s to t = 500 s. The green curve of OCP is higher than those of EVDSM and DMSEM.

As Figure 8 shows, the bars corresponding to the three solutions keep a rising trend with various speed ranges of nodes. The red bars of EVDSM keep the slow rise trend from the range [1, 5] to [10, 15] and have a fast increase from the range [10, 15] to [25, 30]. The orange bars of DMSEM have a slow rise from the range [1, 5] to [10, 15] and a fast rise from the range [10, 15] to [15, 20] and have a stable trend from the range [15, 20] to [20, 25] and have a fast rise from the range [20, 25] to [25, 30]. The green bars of OCP also have a fast rise from the range [1, 5] to [10, 15] and have a fast increase from the range [10, 15] to [25, 30].

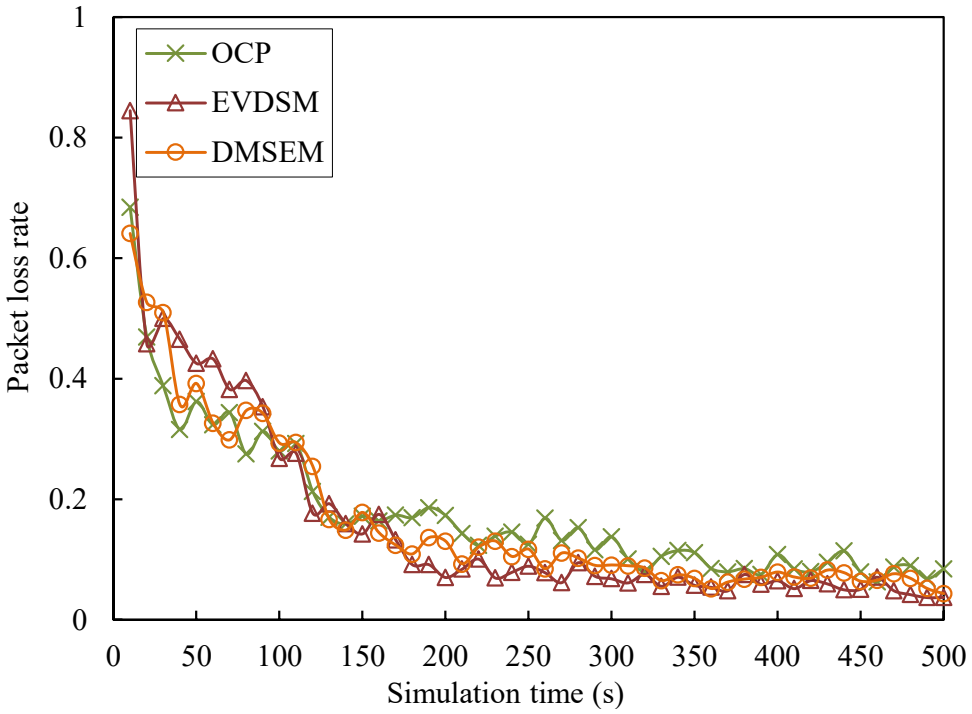

Figure 7. Packet loss rate against simulation time.

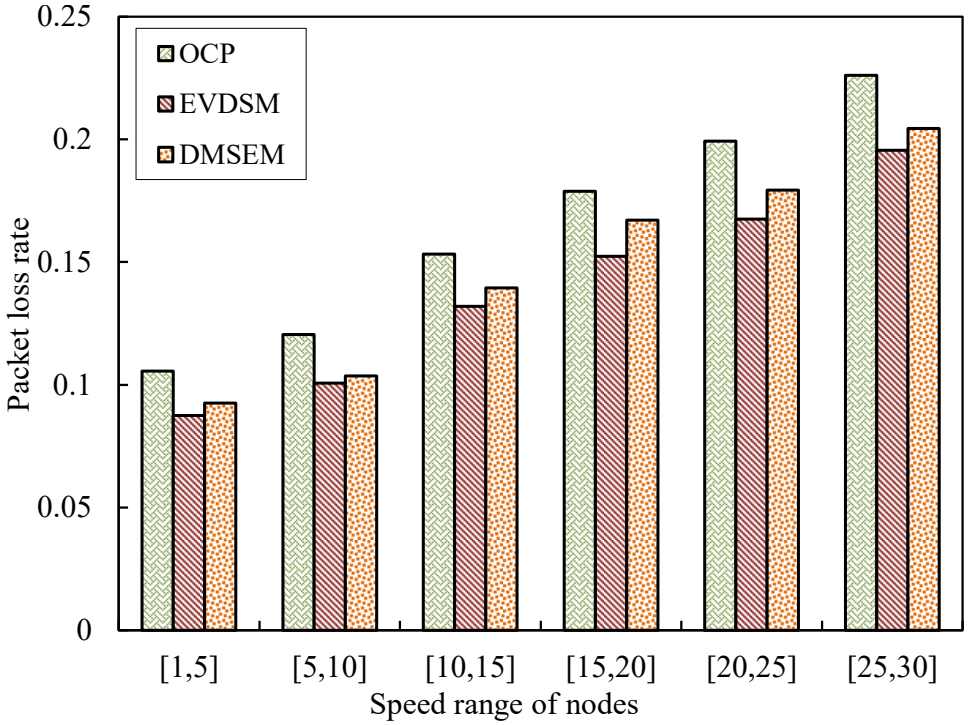

Figure 8. Packet loss rate against various speed ranges of nodes.

EVDSM makes use of data transmission and the stability level of path structure to estimate variation levels of node mobility based on analysis of historical transmission traces of video data. EVDSM considers the available bandwidth and packet loss for the measurement of the performance of data transmission. EVDSM estimates structure stability levels of the data transmission path in terms of investigation of the duration time of the one hop relationship between all adjacent nodes based on the geographical location of nodes. EVDSM effectively reduces the influence of path variation of data transmission

brought by node mobility. Although the path variation caused by the mobility of nodes results in the loss of video data, EVDSM depends on the measurement of data transmission and the stability level of path structure to effectively reduce increment of PLR values with an increasing movement speed of nodes. Therefore, the PLR values of EVDSM are lower than those of DMSEM and OCP. To ensure the stability of the data transmission path and reduce negative influence caused by node mobility, DMSEM clusters encounter events that have similar encounter duration and variation of geographical distance in terms of historical encounter records to classify encounter events, which dynamically pair D2D communication parties in terms of integrating degree between predicted encounter duration and requirement of data transmission time. To recognize and predict encounter events, DMSEM extracts the encounter patterns from the encounter clusters and designs a recognition method for encounter events. The encounter-based D2D communications support high-efficiency data transmission in DMSEM. Although the PLR values of DMSEM keep the rising trend, the increment of PLR values of DMSEM also keeps low levels. OCP does not have the handling method of node mobility and measurement method of data transmission performance, the PLR values of OCP are negatively influenced by the increasing node mobility. Therefore, the ADTD values of OCP are larger than those of EVDSM and DMSEM.

Average freeze time (AFT): The interruption interval time in the process of video playback of users is used to denote the freeze time. The average freeze time is the ratio between the total sum of freeze time and the number of freezes during a period t. The AFT values for every t = 10 s are shown in Figure 9.

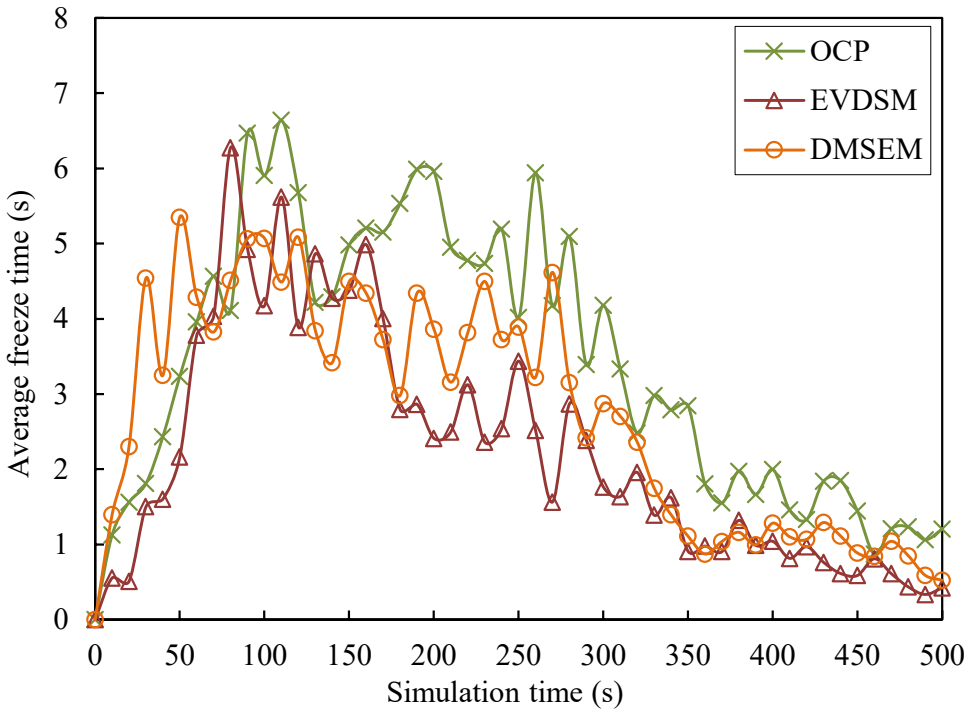

Figure 9. Average freeze time against simulation time.

As Figure 9 shows, the three solutions keep a fall trend after a fast rise with severe fluctuations during the whole simulation time. The red curve of EVDSM has a fast rise from t = 0 s to t = 70 s, keeps high levels from t = 80 s to t = 160 s, experiences a stable fall from t = 350 s to t = 500 s after a fast fall t = 170 s to t = 340 s. The red curve of GSVD keeps the lower levels than those of DMSEM and OCP at the most of simulation time. The orange curve of DMSEM has a fast rise from t = 0 s to t = 30 s, keeps high levels from t = 30 s to t = 280 s, experiences a fast fall from t = 290 s to t = 360 s and has a stable fall from t = 370 s to t = 500 s. The green curve of OCP has a fast fall from t = 0 s to t = 90 s, keeps high levels

from t = 100 s to t = 270 s, has a fast fall from t = 280 s to t = 360 s and experiences a slow decrease from t = 370 s to t = 500 s. The AFT values of OCP are larger than those of EVDSM and DMSEM and have a larger peak value than those of EVDSM and DMSEM.

As Figure 10 shows, the bars corresponding to the three solutions all have a rising trend with the variation of the speed range of nodes. The red bars of EVDSM have a slight increase from the speed range of nodes [1, 5] to [10, 15] and have a slow rise from [15, 20] to [25, 30]. The orange bars of DMSEM have a fast increase from the range [1, 5] to [5, 10], have a slight increase from the range [5, 10] to [10, 15], and have a slow rise from [15, 20] to [25, 30]. The green bars of OCP have a slow rise from the range [1, 5] to [15, 20] and experience a fast rise from the range [20, 25] to [25, 30]. The AFT values of EVDSM are less than those of DMSEM and OCP.

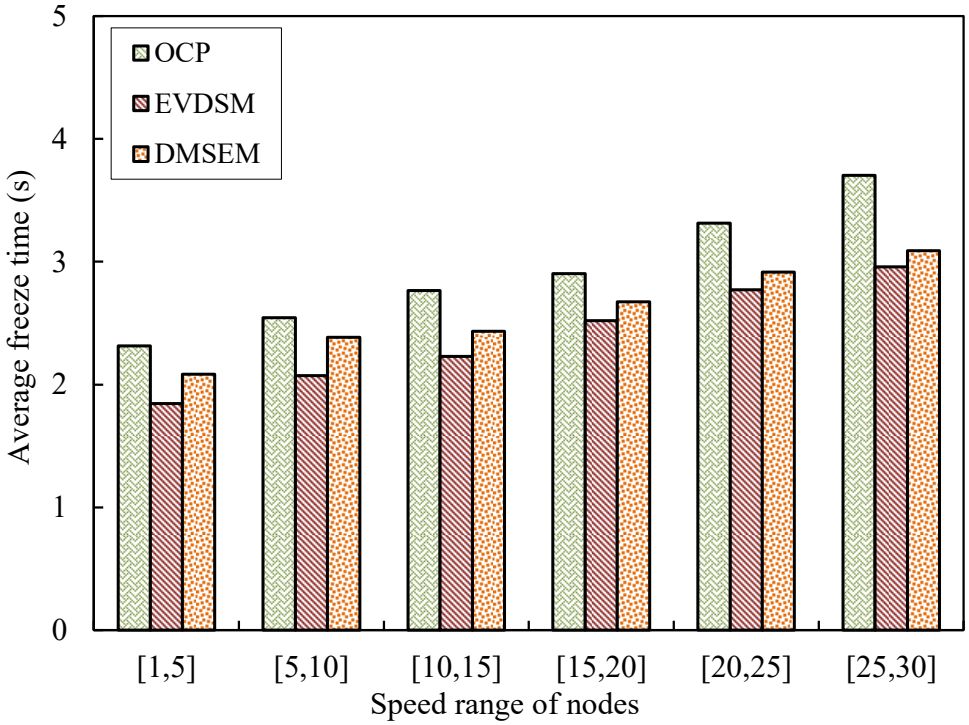

Figure 10. Average freeze time against various speed ranges of nodes.

Video data loss is the main factor of playback interruption. The long interruption time results in a low quality of user experience. EVDSM investigates data transmission and the stability level of path structure to ensure transmission performance of video data by measurement of available bandwidth and packet loss and estimation of duration time of the one hop relationship between all nodes in the data transmission path based on geographical location. The stable paths of data transmission help EVDSM obtain low PLR values, which effectively reduces video data loss and decreases AFT values. Therefore, the AFT values of EVDSM are lower than those of DMSEM and OCP. DMSEM classifies encounter events according to similarities of encounter duration and variation of geographical distance by analysis of historical encounter records, which ensures stable pairing of D2D communication parties and reduces negative influence caused by node mobility. Even if the movement speed of nodes increases, the increment of AFT values of DMSEM also is kept at low levels. Therefore, DMSEM has a similar performance to AFT values. Because OCP does not have the handling method of node mobility and measurement method of data transmission performance, the PLR values of OCP are negatively influenced by the increasing node mobility. Therefore, the AFT values of OCP are larger than those of EVDSM and DMSEM.

Peak signal-to-noise ratio (PSNR): The video quality is denoted by the peak signal-to-noise ratio (PSNR) which is measured in decibels (dB) [51]. The value of PSNR see the formula (26).

$$PSNR = 20 \cdot log_{10}(\frac{MAX\_Bit}{\sqrt{(EXP\_Thr - CRT\_Thr)^2}}). \quad (26)$$

EXP_Thr and CRT_Thr are the expected and real throughput, respectively. MAX_Bit is the maximum value of the transmission rate.

As Figure 11 shows, the three solutions have a fall trend with the increasing speed of nodes. The bars corresponding to EVDSM, DMSEM, and OCP have a slow fall from the range [1, 5] to [5, 10] and experience a slow fall from [10, 15] to [25, 30]. The PSNR bars of EVDSM are higher than those of DMSEM and OCP.

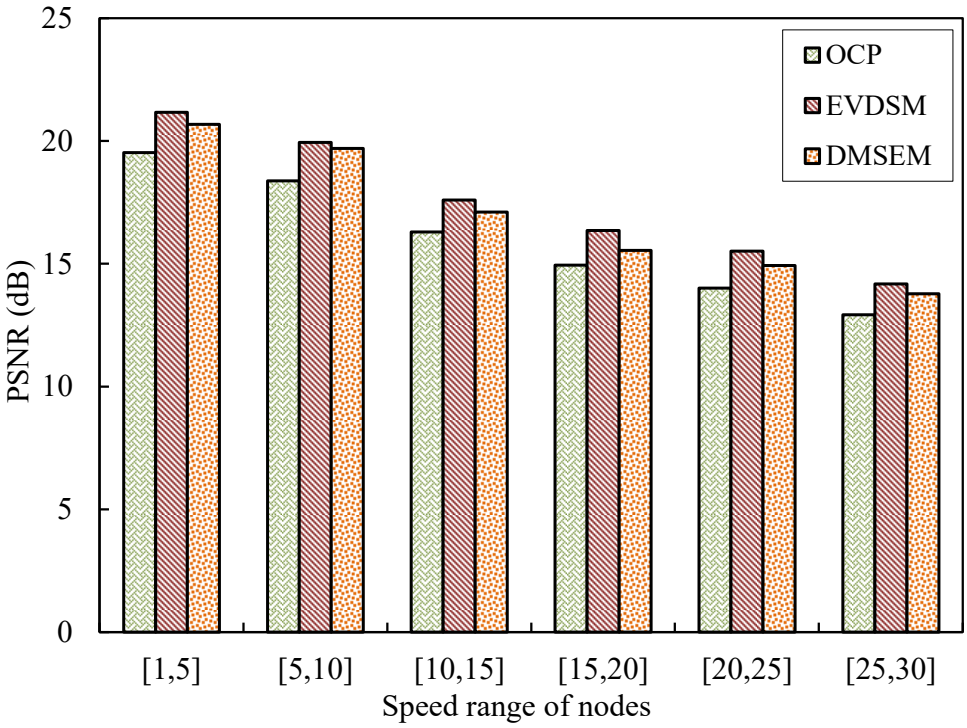

Figure 11. PSNR against various speed ranges of nodes.

The PLR is the main influence factor for the values of PSNR. EVDSM makes use of measurement of data transmission and stability level of path structure to effectively reduce increment of PLR values with an increasing movement speed of nodes. The PSNR performance of EVDSM is better than those of DMSEM and OCP. DMSEM investigates variation levels of geographical distance and encounter duration to reduce the negative influence of node mobility for data transmission performance so that the PLR values of DMSEM can keep the low levels and the negative influence caused by the increase of node movement speed for the PLR values is effectively reduced. DMSEM also obtains relatively high PSNR values. DMSEM has a similar performance to PSNR. Because OCP does not have the handling method of node mobility or the measurement method of data transmission performance, the PLR values of OCP are larger than those of EVDSM and DMSEM. Therefore, the PSNR values of OCP are less than those of EVDSM and DMSEM.

6. Conclusions

In this paper, we propose a Novel Epidemic-based Video Diffusion strategy using awareness of Sociality and Mobility in wireless networks (EVDSM). EVDSM constructs a video diffusion model by investigating interest preference, social influence, and mobility and defines the four roles of video-sharing users in social networks according to the Epidemic model. EVDSM uses the content-based similarity between watched and popular

videos and the discrimination between user preference and popular videos to estimate the interest levels of users. EVDSM uses the weight value of social edges, the push success rate, and the influence levels of neighbor nodes to estimate the social influence levels of users. EVDSM defines an estimation method of user roles according to interest preference and social influence and an identification method of user roles in terms of the video-sharing behaviors of users. EVDSM uses the expected time length of data transmission and the stability level of path structure to estimate user mobility levels. EVDSM defines the priority levels of pairing between infectors and candidate infectors according to the joint optimization of pairing success rate and video delivery performance, which promotes the effectiveness of video sharing and ensures user QoE. The simulation results show that EVDSM obtains a lower startup delay, a lower average data transmission delay, a lower packet loss rate, a lower average freeze time, and a higher peak signal-to-noise ratio than DMSEM and OCP.

Author Contributions: Writing—original draft preparation S.J., writing—review and literature search R.Z., writing—review and data analysis X.S., writing—review and data curation L.L. All authors have read and agreed to the published version of the manuscript.

Funding: This research was funded by the Training Plan for Young Backbone Teachers of Colleges and Universities in Henan under Grant nos. 2020GGJS191, Special project of key research and development Plan of Henan Province under Grant nos. 221111111700, the Innovation Team of University Science and Technology of Henan Province under Grant nos. 22IRTSTHN016 and 23IRTSTHN017, and the National Natural Science Foundation of China (NSFC) under Grant Nos. 42071198.

Data Availability Statement: Not applicable.

Conflicts of Interest: The authors declare that there is no conflict of interest regarding the publication of this paper.

Abbreviations

Abbreviations	Descriptions
EVDSM	Epidemic-based Video Diffusion strategy using awareness of Sociality and Mobility in wireless networks
PLR	Packet Loss Rate
QoE	Quality of Experience
CSQCA	Collaborative Social-aware QoE-driven video Caching and Adaption framework
P2P	Peer-to-Peer
NS-3	Network Simulator 3
APs	Access Points
FPLM	Friis Propagation Loss Model
SD	Startup Delay
ADTD	Average Data Transmission Delay
AFT	Average Freeze Time
PSNR	Peak Signal-to-Noise Ratio

References

1. Lv, Z.; Qiao, L.; You, I. 6G-Enabled Network in Box for Internet of Connected Vehicles. *IEEE Trans. Intell. Transp. Syst.* **2021**, *22*, 5275–5282. [CrossRef]
2. Al-Zubi, R.T.; Darabkh, K.A.; Khattabi, Y.M.; Issa, M.T.A. Markov-based analysis for cooperative HARQ-aided NOMA transmission scheme in 5G and beyond. *Trans. Emerg. Telecommun. Technol.* **2022**, *33*, e4444. [CrossRef]
3. Tejasvi, T.R.; Manjaiah, D.H. Energy and spectral efficient resource allocation in 5G HetNet using optimized deep bi-BRLSTM model. *Trans. Emerg. Telecommun. Technol.* **2022**, *33*, e4471. [CrossRef]
4. Noor-A-Rahim, M.; Liu, Z.; Lee, H.; Khyam, M.O.; He, J.; Pesch, D.; Moessner, K.; Saad, W.; Poor, H.V. 6G for Vehicle-to-Everything (V2X) Communications: Enabling Technologies, Challenges, and Opportunities. *Proc. IEEE* **2022**, *110*, 712–734. [CrossRef]
5. Zhong, L.; Chen, X.; Xu, C.; Ma, Y.; Wang, M.; Zhao, Y.; Muntean, G. A Multi-User Cost-Efficient Crowd-Assisted VR Content Delivery Solution in 5G-and-Beyond Heterogeneous Networks. *IEEE Trans. Mob. Comput.* **2022**. [CrossRef]
6. Osaghae, E.N.; Misra, S.; Ahuja, R.; Koyuncu, M. Particle swarm optimization of the spectral and energy efficiency of an SCMA-based heterogeneous cellular network. *Trans. Emerg. Telecommun. Technol.* **2022**, *33*, e4508.

7. Jubran, M.; Abbas, A.; Andreopoulos, Y. Sequence-Level Reference Frames in Video Coding. *IEEE Trans. Circuits Syst. Video Technol.* **2022**, *32*, 1578–1591. [CrossRef]
8. Xu, C.; Qin, J.; Zhang, P.; Gao, K.; Grieco, L.A. Reinforcement Learning-based Mobile AR/VR Multipath Transmission with Streaming Power Spectrum Density Analysis. *IEEE Trans. Mob. Comput.* **2022**. *21*, 4529–4540. [CrossRef]
9. Roy, A.; De, P.; Saxena, N. Location-based social video sharing over next generation cellular networks. *IEEE Commun. Mag.* **2015**, *53*, 136–143. [CrossRef]
10. Pelau, C.; Pop, M.-I.; Stanescu, M.; Sanda, G. The Breaking News Effect and Its Impact on the Credibility and Trust in Information Posted on Social Media. *Electronics* **2023**, *12*, 423. [CrossRef]
11. Faragallah, O.S.; El-Sayed, H.S.; El-Mashed, M.G. High mobility transmission system under intelligent reflecting surface. *Trans. Emerg. Telecommun. Technol.* **2022**, *33*, e4495. [CrossRef]
12. Chowdhury, M.Z.; Hasan, M.K.; Sahjalal, M.; Hossan, M.T.; Jang, Y.M. Optical Wireless Hybrid Networks: Trends, Opportunities, Challenges, and Research Directions. *IEEE Commun. Surv. Tutor.* **2020**, *22*, 930–966. [CrossRef]
13. Moses, M.L.; Ramkumarraja, M. An integrated AHP-ELECTRE and deep reinforcement learning methods for handover performance optimization in an LTE-A networks. *Trans. Emerg. Telecommun. Technol.* **2022**, *33*, e4536. [CrossRef]
14. Xu, Y.; Gu, B.; Hu, R.Q.; Li, D.; Zhang, H. Joint Computation Offloading and Radio Resource Allocation in MEC-Based Wireless-Powered Backscatter Communication Networks. *IEEE Trans. Veh. Technol.* **2021**, *70*, 6200–6205. [CrossRef]
15. Baltaci, A.; Dinc, E.; Ozger, M.; Alabbasi, A.; Cavdar, C.; Schupke, D. A Survey of Wireless Networks for Future Aerial Communications (FACOM). *IEEE Commun. Surv. Tutor.* **2021**, *23*, 2833–2884. [CrossRef]
16. Xiao, H.; Xu, C.; Ma, Y.; Yang, S.; Zhong, L.; Muntean, G.M. Edge Intelligence: A Computational Task Offloading Scheme for Dependent IoT Application. *IEEE Trans. Wirel. Commun.* **2022**, *21*, 7222–7237. [CrossRef]
17. Yan, H.; Lin, T.-H.; Zeng, M.; Wu, J.; Li, Y.; Jin, D. Discovering Usage Patterns of Mobile Video Service in the Cellular Networks. *IEEE Trans. Netw. Serv. Manag.* **2021**, *18*, 1789–1802. [CrossRef]
18. Tan, Z.; Dong, F.; Liu, X.; Li, C.; Nie, X. VMLH: Efficient Video Moment Location via Hashing. *Electronics* **2023**, *12*, 420. [CrossRef]
19. Wu, D.; Bao, R.; Li, Z.; Wang, H.; Zhang, H.; Wang, R. Edge-Cloud Collaboration Enabled Video Service Enhancement: A Hybrid Human-Artificial Intelligence Scheme. *IEEE Trans. Multimed.* **2021**, *23*, 2208–2221. [CrossRef]
20. Chou, Y.-F.; Huang, H.-H.; Cheng, R.-G. Modeling Information Dissemination in Generalized Social Networks. *IEEE Commun. Lett.* **2013**, *17*, 1356–1359. [CrossRef]
21. Chen, Z.; Taylor, K. Modeling the Spread of Influence for Independent Cascade Diffusion Process in Social Networks. In Proceedings of the 2017 IEEE 37th International Conference on Distributed Computing Systems Workshops (ICDCSW), Atlanta, GA, USA, 5–8 June 2017.
22. Yang, Y.; Lu, Z.; Li, V.O.K.; Xu, K. Noncooperative Information Diffusion in Online Social Networks Under the Independent Cascade Model. *IEEE Trans. Comput. Soc. Syst.* **2017**, *4*, 150–162. [CrossRef]
23. Prasse, B.; Mieghem, P.V. Network Reconstruction and Prediction of Epidemic Outbreaks for General Group-Based Compartmental Epidemic Models. *IEEE Trans. Netw. Sci. Eng.* **2020**, *7*, 2755–2764. [CrossRef]
24. Yang, W.; Qin, Y.; Yang, Y. Characterizing the Multicast Nature of Malicious Flows in CCN via SIS Epidemic Model. *IEEE Syst. J.* **2022**, *16*, 2240–2250. [CrossRef]
25. Moon, S.A.; Sahneh, F.D.; Scoglio, C. Group-Based General Epidemic Modeling for Spreading Processes on Networks: GroupGEM. *IEEE Trans. Netw. Sci. Eng.* **2021**, *16*, 434–446. [CrossRef]
26. Song, J.; Yang, F.; Zhang, W.; Ma, Z. Parametric Model for Video Streaming Services With Different Spatial and Temporal Resolutions. *IEEE Trans. Circuits Syst. Video Technol.* **2021**, *31*, 3380–3390. [CrossRef]
27. Shang, Z.; Ebenezer, J.P.; Wu, Y.; Wei, H.; Sethuraman, S.; Bovik, A.C. Study of the Subjective and Objective Quality of High Motion Live Streaming Videos. *IEEE Trans. Image Process.* **2022**, *31*, 1027–1041. [CrossRef] [PubMed]
28. Hu, J.; Liao, X.; Wang, W.; Qin, Z. Detecting Compressed Deepfake Videos in Social Networks Using Frame-Temporality Two-Stream Convolutional Network. *IEEE Trans. Circuits Syst. Video Technol.* **2022**, *32*, 1089–1102. [CrossRef]
29. Chiang, Y.; Hsu, C.-H.; Wei, H.-Y. Collaborative Social-Aware and QoE-Driven Video Caching and Adaptation in Edge Network. *IEEE Trans. Multimed.* **2021**, *23*, 4311–4325. [CrossRef]
30. Hu, H.; Wen, Y.; Feng, S. Budget-Efficient Viral Video Distribution Over Online Social Networks: Mining Topic-Aware Influential Users. *IEEE Trans. Circuits Syst. Video Technol.* **2018**, *28*, 759–771. [CrossRef]
31. Zhang, X.; Wei, X.; Zhou, L.; Qian, Y. Social-Content-Aware Scalable Video Streaming in Internet of Video Things. *IEEE Internet Things J.* **2022**, *9*, 830–843. [CrossRef]
32. Hsu, T.-H.; Tung, Y.-M. A Social-Aware P2P Video Transmission Strategy for Multimedia IoT Devices. *IEEE Access* **2020**, *8*, 95574–95584. [CrossRef]
33. Langa, S.F.; Climent, M.M.; Cernigliaro, G.; Rivera, D.R. Toward Hyper-Realistic and Interactive Social VR Experiences in Live TV Scenarios. *IEEE Trans. Broadcast.* **2022**, *68*, 13–32. [CrossRef]
34. Cao, Y.; Jiang, T.; Chen, X.; Zhang, J. Social-Aware Video Multicast Based on Device-to-Device Communications. *IEEE Trans. Mob. Comput.* **2016**, *15*, 1528–1539. [CrossRef]
35. Hu, H.; Wen, Y.; Chua, T.-S.; Huang, J.; Zhu, W.; Li, X. Joint Content Replication and Request Routing for Social Video Distribution Over Cloud CDN: A Community Clustering Method. *IEEE Trans. Circuits Syst. Video Technol.* **2016**, *26*, 1320–1333. [CrossRef]

36. Fan, Y.; Yang, B.; Hu, D.; Yuan, X.; Xu, X. Social- and Content-Aware Prediction for Video Content Delivery. *IEEE Access* **2020**, *8*, 29219–29227. [CrossRef]
37. Zhang, R.; Jia, S.; Ma, Y.; Xu, C. Social-Aware D2D Video Delivery Method Based on Mobility Similarity Measurement in 5G Ultra-Dense Network. *IEEE Access* **2020**, *8*, 52413–52427. [CrossRef]
38. Wang, Z.; Liu, J.; Zhu, W. Social-aware video delivery: Challenges, approaches, and directions. *IEEE Netw.* **2016**, *30*, 35–39. [CrossRef]
39. Kilanioti, I. Improving Multimedia Content Delivery via Augmentation With Social Information: The Social Prefetcher Approach. *IEEE Trans. Multimed.* **2015**, *17*, 1460–1470. [CrossRef]
40. Rajapaksha, P.; Farahbakhsh, R.; Mohammadi, S.; Dailey, M.N.; Crespi, N. Video Content Delivery Enhancement in CDNs Based on Users' Social Information. In Proceedings of the 2016 IEEE Globecom Workshops (GC Wkshps), Washington, DC, USA, 4–8 December 2016.
41. Niu, G.; Fan, X.; Li, V.O.; Long, Y.; Xu, K. Multi-Source-Driven Asynchronous Diffusion Model for Video-Sharing in Online Social Networks. *IEEE Trans. Multimed.* **2014**, *16*, 2025–2037. [CrossRef]
42. Long, Y.; Li, V.O.; Niu, G. Modeling video viewing and sharing behaviors in online social networks. In Proceedings of the 2015 IEEE International Conference on Communications (ICC), London, UK, 8–12 June 2015.
43. Jiao, J.; Guo, S.; Wang, Y.; Yang, Y. Energy-Efficient Cooperative Scalable Video Distribution and Sharing in Mobile Social Networks. In Proceedings of the 15th International Conference on Mobile Ad-Hoc and Sensor Networks, Shenzhen, China, 11–13 December 2019.
44. Hu, B.; Cheung, G.; Zhao, H.V. Incentive analysis for cooperative distribution of interactive multiview video. In Proceedings of the 2012 IEEE International Conference on Acoustics, Speech and Signal, Kyoto, Japan, 25–30 March 2012.
45. Wu, D.; Liu, Q.; Wang, H.; Yang, Q.; Wang, R. Cache Less for More: Exploiting Cooperative Video Caching and Delivery in D2D Communications. *IEEE Trans. Multimed.* **2019**, *21*, 1788–1798. [CrossRef]
46. Xu, C.; Wang, M.; Chen, X.; Zhong, L.; Grieco, L.A. Optimal information centric caching in 5G device-to-device communications. *IEEE Trans. Mob. Comput.* **2018**, *17*, 2114–2126. [CrossRef]
47. Li, W. Random texts exhibit Zipfs-law-like word frequency distribution. *Inst. Electr. Electron. Eng. Trans. Inf. Theory* **1992**, *38*, 1842–1845.
48. Li, Q.; Zhang, Y.; Pandharipande, A.; Ge, X.; Zhang, J. D2D-Assisted Caching on Truncated Zipf Distribution. *IEEE Access* **2019**, *7*, 13411–13421. [CrossRef]
49. Aldalbahi, A.; Rahaim, M.; Khreishah, A.; Ayyash, M.; Little, T.D.C. Visible Light Communication Module: An Open Source Extension to the ns3 Network Simulator With Real System Validation. *IEEE Access* **2017**, *5*, 22144–22158. [CrossRef]
50. Zhang, H.; Liao, Y.; Song, L. D2D-U: Device-to-Device Communications in Unlicensed Bands for 5G System. *IEEE Trans. Wirel. Commun.* **2017**, *16*, 3507–3519.
51. Lee, S.B.; Muntean, G.M.; Smeaton, A.F. Performance-aware replication of distributed pre-recorded IPTV content. *IEEE Trans. Broadcast.* **2009**, *55*, 516–526.